INTERFACE

royalsocietypublishing.org/journal/rsif

Research

Cite this article: Steinbach G, Crisan C, Ng SL, Hammer BK, Yunker PJ. 2020 Accumulation of dead cells from contact killing facilitates coexistence in bacterial biofilms. *J. R. Soc. Interface* **17**: 20200486.
https://doi.org/10.1098/rsif.2020.0486

Received: 18 June 2020
Accepted: 12 November 2020

Subject Category:
Life Sciences–Physics interface

Subject Areas:
biophysics

Keywords:
bacteria, emergence, antagonism

Author for correspondence:
Peter J. Yunker
e-mail: peter.yunker@physics.gatech.edu

Electronic supplementary material is available online at https://doi.org/10.6084/m9.figshare.c.5228072.

THE ROYAL SOCIETY PUBLISHING

Accumulation of dead cells from contact killing facilitates coexistence in bacterial biofilms

Gabi Steinbach[1,2], Cristian Crisan[2,3,4], Siu Lung Ng[2,3,4], Brian K. Hammer[2,3,4] and Peter J. Yunker[1,2,4]

[1]School of Physics, [2]Center for Microbial Dynamics and Infection, [3]School of Biological Sciences, and [4]Institute for Bioengineering and Biosciences, Georgia Institute of Technology, Atlanta, GA, USA

PJY, 0000-0001-8471-4171

Bacterial communities are governed by a wide variety of social interactions, some of which are antagonistic with potential significance for bacterial warfare. Several antagonistic mechanisms, such as killing via the type VI secretion system (T6SS), require killer cells to directly contact target cells. The T6SS is hypothesized to be a highly potent weapon, capable of facilitating the invasion and defence of bacterial populations. However, we find that the efficacy of contact killing is severely limited by the material consequences of cell death. Through experiments with *Vibrio cholerae* strains that kill via the T6SS, we show that dead cell debris quickly accumulates at the interface that forms between competing strains, preventing physical contact and thus preventing killing. While previous experiments have shown that T6SS killing can reduce a population of target cells by as much as 10^6-fold, we find that, as a result of the formation of dead cell debris barriers, the impact of contact killing depends sensitively on the initial concentration of killer cells. Killer cells are incapable of invading or eliminating competitors on a community level. Instead, bacterial warfare itself can facilitate coexistence between nominally antagonistic strains. While a variety of defensive strategies against microbial warfare exist, the material consequences of cell death provide target cells with their first line of defence.

1. Introduction

Bacteria commonly inhabit biofilms in the form of crowded, surface-attached microbial consortia embedded within a viscous matrix of polymers. Interactions between different bacterial strains and species govern the spatial organization and composition of biofilms [1–3], and ultimately affect the proliferation and survival of individual strains. These interactions can turn deadly. Bacteria have evolved many mechanisms to kill each other within biofilms [4,5], many of them requiring direct contact between cells [4,6–9]. One such contact killing mechanism is the broadly prevalent type VI secretion system (T6SS) in Gram-negative bacteria [10]. A significant amount of work has produced a detailed picture of the T6SS. Details are emerging of the T6SS structure, toxins and regulation [10–20]. However, the importance of this lethal activity in natural communities remains unclear [21,22]. Experiments have primarily focused on the outcome of competitions between T6SS-proficient 'killers' and target strains that lack T6SS activity, but the dynamics of T6SS killing are much less studied [23] (though dynamic simulations have made a number of successful predictions [24–28]). Understanding the impact of the T6SS requires experimental observation of contact killing in microbial communities as a function of time and isolated from other factors. This is a crucial step in assessing the ecological role of contact killing over short and long time scales.

T6SS-mediated killing is widely considered a potent weapon. In biofilms grown from a mixture of T6SS-proficient bacteria and target strains on planar agar pads, killer cells decreased the abundance of target cells by as much as 10^6-fold within 3 h [15,23,29–31]. Based on these competition assays, the T6SS

is hypothesized to play important roles in inter- and intra-strain competition; for example, facilitating invasion of colonized space, elimination of competitors and defence against invaders and cheaters in biofilms [21,28,32–34]. However, in these competition assays T6SS-mediated killing is rarely able to completely eliminate all susceptible target cells, even when killer cells start at a numerical advantage (a 10 : 1 number ratio of killer : target cells is often used) [23,24,30,31,35]. Further, while the killing rate is typically very high shortly after inoculating competing strains on agar pads, killing nearly halts a few hours later, despite the presence of target cells [23]. This dramatic decrease in killing occurs even when the killer strain expresses a constitutively active T6SS [23]. While some studies report defence mechanisms that mitigate or counteract T6SS attacks [36–41], it is difficult to isolate alterations in T6SS activity over time as developing biofilms become increasingly heterogeneous [42,43] and constantly change [44–48]: biomass increases, nutrient and oxygen concentrations drop, excreted waste products accumulate and cellular behaviour changes owing to signalling from secreted public goods. As a result, a detailed picture of how T6SS killing proceeds within biofilms and how T6SS-mediated killing rates change over time remains elusive.

Here, we present the spatio-temporal dynamics of T6SS-mediated killing. We used the T6SS-proficient killer strain *Vibrio cholerae* C6706 and mutants of it, which secrete lethal effectors that cause cell death [30,35,37,49–51]. Through microscopy experiments, we show that while T6SS-mediated killing is effective on first contact between competing strains, surprisingly, killing nearly ceases after a few hours because of the accumulation of dead cell debris. Contact killing experiments typically focus on living cells as they measure the number of surviving target cells after a certain time of inoculation [15,29–31,39,52–55]. This approach was fundamental in discovering the deadly effect of T6SS [7], the characteristic spatial structure that emerges from contact killing [2,24,26,28], and microbial defence strategies against T6SS attacks [36–39]. Here, we focus on the role of dead cells and dead cell debris. We confirm that dead cell debris accumulates at the interface between competing strains and eventually prevents contact, thus halting killing. Paradoxically, contact killing may thus play a protective role in biofilms, facilitating the formation and coexistence of separate clonal domains [56,57].

2. Results

To study how T6SS killing proceeds within biofilms, we optically recorded the spatio-temporal dynamics of biofilms comprising two engineered strains of *V. cholerae*, a model organism for studying the T6SS [7]. These strains are isogenic, and only differ in their T6SS toxins and immunity modules, their ability to express T6SS and their fluorescent proteins [24]. To isolate the effects of killing from other effects related to changes in biofilm height (which can impact cellular behaviour [43]), we grew biofilms in confinement between a lysogeny broth (LB) agar pad and a glass coverslip (figure 1*a*), which limited vertical growth to less than 6 µm. (See electronic supplementary material for details on strains and sample preparation.)

2.1. Spatio-temporal dynamics

As a first step, using confocal time-lapse microscopy we investigated the temporal dynamics of unidirectional killing: the killer was a T6SS-proficient (T6SS+) *V. cholerae* strain, while the target was a susceptible, T6SS-defective (T6SS–) *V. cholerae* strain. We observed the formation of clonal domains (figure 1*b*) upon reproduction and killing. This phenomenon is reminiscent of domain formation observed in populations of mutual killer strains (i.e. both strains are T6SS+) [24], even though in our experiments one strain—the target strain—was engineered to be defective at T6SS killing. While we observed that domains of the killer strain expanded quickly at early times, domain growth later slowed substantially (figure 1*b*). We quantified the temporal dynamics of mixed populations of killer and target strains (figure 1*c*) by measuring the relative abundance of the fluorescent killer strain in the microscopy images over 15 h, for four different initial ratios of killer and target cells (see electronic supplementary material for further

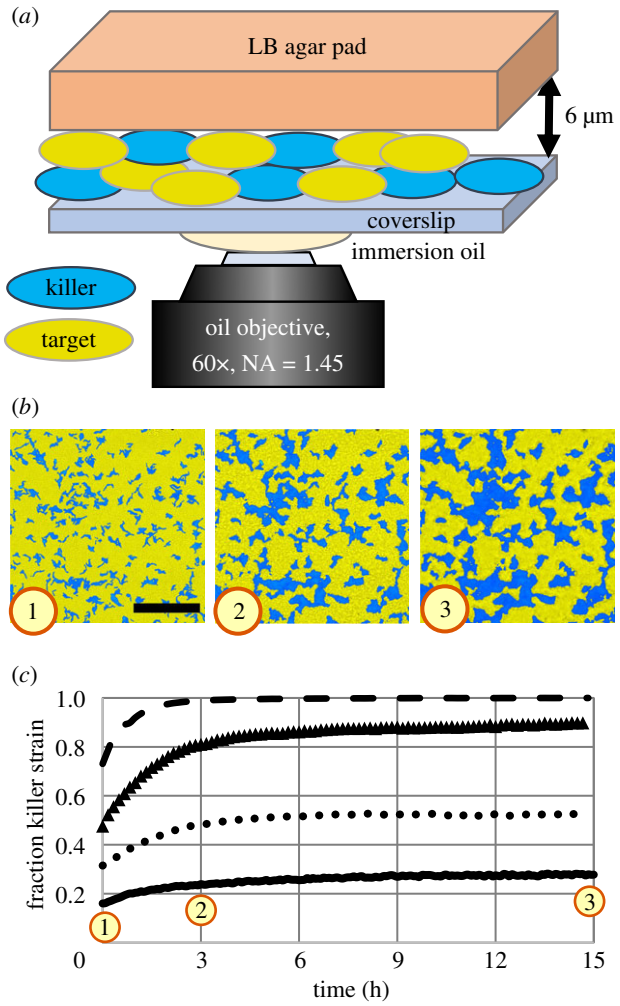

Figure 1. Contact killing slows substantially over time. (*a*) Cartoon depiction of biofilm samples for imaging. Confinement between an agar pad and a glass coverslip leads to a maximum biofilm thickness of approximately 6 µm. (*b*) Fluorescence images of a unidirectional competition between killer cells (blue) and target cells (yellow) at 0 h, 3 h and 15 h (left to right, respectively). The initial relative abundances were 0.09 killer cells and 0.91 target cells. T6SS-mediated contact killing leads to the formation of clonal domains, which increase in size over time. Scale bar: 50 µm. (*c*) Relative abundance of the killer cells over time for four different initial conditions (killer cell relative abundance during inoculation: 0.5 (dashed line), 0.33 (triangles), 0.17 (dotted line) and 0.09 (solid line)) measured from time-lapse images as depicted in (*b*). In all cases, the relative abundance of killer cells initially increased quickly, followed by a substantially slower increase after 3 h. (See also electronic supplementary material, video 1.)

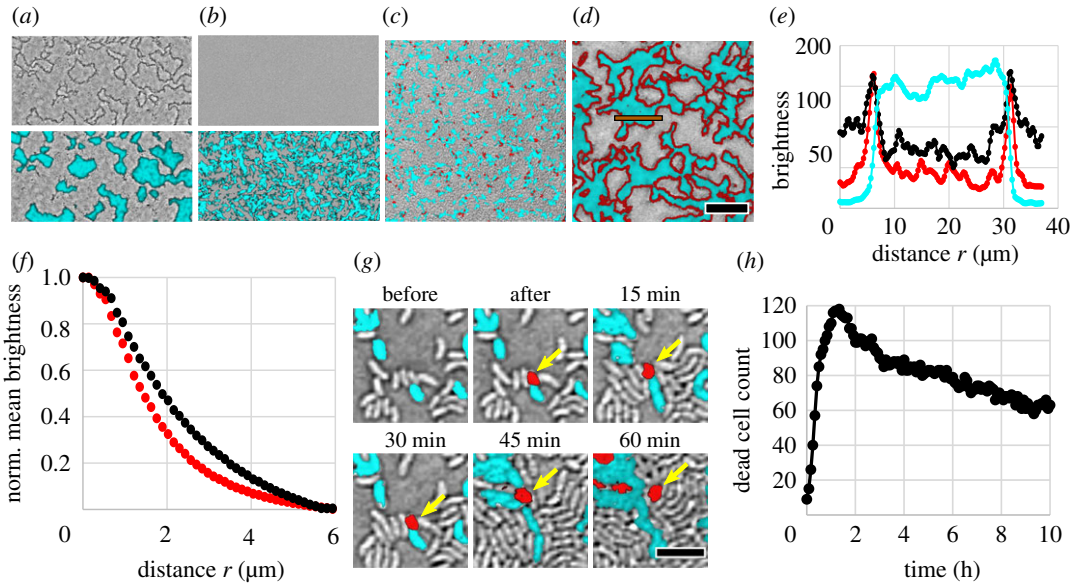

Figure 2. Characterization of dead cell debris. (*a*) Representative bright-field image alone (top) and overlaid with fluorescence channel (bottom) of biofilms exhibiting unidirectional killing, recorded after 7 h of growth. Killer cells express superfolder green fluorescent protein (sfGFP) (cyan) while target cells are unlabelled. The entire field of view is densely packed with bacteria. (*b*) Same as (*a*) but the killer strain is engineered to be T6SS-deficient; no T6SS killing occurs and dark outlines are absent. (*c*,*d*) Merged bright-field and fluorescence images of unidirectional killing at start (0 h) (*c*) and after 7 h (*d*). Again, the killer expresses sfGFP (visible as cyan) while the target is unlabelled (grey). The DNA of compromised cells, i.e. dead cell debris, is labelled red via PI. Scale bar (*a*–*d*): 30 µm. (*e*) Intensity profile of different microscope images across a clonal patch (integrated vertically over the orange box in (*d*)) in the fluorescence images and bright-field image (inverted grey scale). (*f*) Normalized mean intensity of PI signal (red curve) and inverted bright-field signal (black curve) within a distance *r* from the interface between competing strains in (*d*). (*g*) Killing event, where a fluorescent killer cell kills a non-fluorescent target cell, which subsequently turns red. The dead cell debris is relocated by neighbouring cells that exert forces upon growth. Scale bar: 4 µm. (*h*) Counting the number of discrete PI-labelled cells over time demonstrates that PI-labelled dead cell debris persists long after cell death. Data were recorded from individual target cells densely surrounded by killer cells (initial target to killer number ratio of 1 : 50).

details on image analysis). Note that the mixing ratios do not reflect the relative abundance of killer cells at 0 h. Biofilms were grown from relatively low cell concentrations ($OD_{600} = 1$). However, we began measuring the relative abundance of the fluorescent strain only after a dense cell layer has formed, which we define to be when time = 0 h, after which the vast majority of killing takes place. Killer populations increased their relative abundance from 12% to 42%. In contrast, we performed control experiments with two non-killer strains. When killing was absent, the population of the fluorescent strain changed by less than 3% over 15 h for various mixing ratios (electronic supplementary material, figure S2). Therefore, demographic changes in biofilms with T6SS-active strains can mainly be attributed to killing. In all cases of unidirectional killing, the killer strain initially increased its population rapidly and reached approximately 90% of its final size after approximately 3 h. Killing dramatically slowed afterwards. We observed similar temporal dynamics in experiments with mutually killing *V. cholerae* strains (electronic supplementary material, figure S4a,b and video 1). Again, a transition from rapid killing to almost no killing occurred after approximately 3 h. These observations are consistent with previously reported observations of small but long-lived target populations [23]. Why does T6SS-mediated killing stop after just a few hours?

2.2. Cell debris barrier

Surprisingly, we found that the boundary between competing strains was visible in images recorded with bright-field microscopy (figure 2*a*). Dark outlines become visible in bright-field images (figure 2*a*, top image); these dark outlines align with the interface between domains of killer and target cells in fluorescence images (figure 2*a*, bottom image). Time-lapse images showed that these dark outlines form at early times in biofilms with killing, but they are absent at all times in non-killer biofilms, i.e. those with two isogenic T6SS– strains (electronic supplementary material, figure S3). Small clonal domains still emerged in non-killer biofilms as non-motile, divided cells typically remain close after reproduction (figure 2*b*, bottom image), but the interface between these clonal domains did not appear dark in bright-field images (figure 2*b*, top image). The ability to visualize the interface between competing strains using bright-field microscopy is not expected since the two isogenic strains do not differ in their material properties—including index of refraction—so they appear identical when imaged with bright-field microscopy. The presence of dark lines in biofilms with T6SS killing suggests that there occurred a change in material properties (e.g. index of refraction) at the border between strains. Based on this observation, and the data presented above, we hypothesized that dead cell debris accumulates as cells are killed. Such cell debris may eventually prevent competing cells from contacting. Similar observations have been made previously when studying T6SS-mediated interactions with non-lethal effectors [58–60].

To test our hypothesis, we visualized dead cell debris in growing biofilms with propidium iodide (PI). PI binds to the DNA of cells with a compromised membrane and exhibits high red fluorescence. While stained dead cells appeared throughout the biofilm during the earliest stages of growth when clonal domains are small (figure 2*c*; see also electronic supplementary material, video 2), at later times the dead cell stain was clearly localized at the interface between large

clonal domains (figure 2*d*). The PI signal is well aligned with both the interface between strains and the dark outlines seen with bright-field microscopy (figure 2*e*). The PI signal exhibits a peak at the same position (distance of 6.2 and 31.3 µm) where the cell fluorescence declines to about 30% of its maximum value. From a Gaussian fit we found that both peaks in PI signal and bright-field signal differ in position by less than 0.3 µm and differ in width (i.e. standard deviation of the peak) by less than 0.1 µm. This sub-micron alignment of signals suggests that dark outlines observed via bright-field microscopy correspond to a substantial amount of cell debris at the interfaces between patches.

To quantify the localization of dead cell debris at interfaces throughout the biofilm, we measured the mean intensity of PI signal as a function of distance from the interface between strains (figure 2*f*; see electronic supplementary material for more details on the image analysis). The intensity of the PI signal decays with distance from the strain interface, and reaches half its maximum value at a distance of 1.4 µm. We applied the same image analysis to bright-field images and characterized the dark outlines at the strain interfaces. The dark outlines lead to a similar decaying curve, reaching half its maximum value at a distance of about 1.8 µm (figure 2*f*) or higher, depending on the chosen threshold value during image analysis (electronic supplementary material, figure S1c). Both curves confirm that dead cell debris is highly localized at the interface between strains. Crucially, the estimated dead cell debris layer thickness is larger than the length of a *V. cholerae* cell.

To account for the observed slow rate of killing after 3 h, the dead cell debris that separates competing strains must also be stable over long periods of time. We observed that debris from one individual dead cell remained clearly visible for at least 60 min, even as it was relocated via forces exerted by neighbouring cells as those reproduce and die (figure 2*g*). However, the emergence of more dead cells in close proximity inhibits tracking for longer times.

To quantify the persistence of dead cell material over long times, we mixed 98% T6SS+ killer cells and 2% T6SS− target cells and inoculated at high density ($OD_{600} = 10$), so experiments began with close-packed cellular monolayers. Target cells were very far from each other, allowing us to isolate and track individual stained dead cells over long times (approx. 10 h). All 117 individual target cells died within 1.2 h of inoculation (figure 2*h*), and were tracked by PI labelling afterwards. The number of dead cells with detectable PI signal slowly decreased over time. The decrease in the number of PI-labelled dead cells may be due to a local loss in the presence of dead cell debris, e.g. the material may degrade and diffuse away. Note that the PI-labelled area per dead cell also decreased over time (electronic supplementary material, figure S5), which may be caused by degradation or compaction of dead cell debris. However, despite the observed decrease of dead cell debris, over 80% of dead cells displayed a clear PI signal after 4 h, and the majority of dead cells (over 50%) still displayed a clear PI signal after 10 h. Thus, a substantial amount of dead cell debris persisted over several hours.

We can derive a simple estimate for the time that it takes a dead cell debris barrier to form in our experiments. A single layer of dead cells is sufficient to halt killing. The time it takes a single layer of dead cells to form depends on the kill rate, which we estimate from experiments in which individual target cells are surrounded by killer cells (figure 2*h*). Target cells died after $\tau = 0.43 \pm 0.02$ h on average ($N = 117$ individual target cells). In a random, close-packing of non-spherical cells, each cell is expected to contact, on average, between $z = 6$ (cell monolayer [61]) and $z = 10$ (three-dimensional [62]) other cells. Assuming that killer cells fire the T6SS apparatus in random directions [11], a contact between killer and target cells leads to a killing event between $z \cdot \tau = 2.58 \pm 0.12$ h and 4.30 ± 0.20 h on average. This time scale agrees with our experimental finding in figure 1*c*.

Accumulation of dead cell debris is also present in competitions between non-isogenic strains. To test the accumulation of debris between non-isogenic strains, we competed the previously used *V. cholerae* killer (T6SS+) against other killer strains (four other environmental isolates of *V. cholerae* [29]) and a non-killer strain (*Vibrio harveyi*) (electronic supplementary material, figure S6). Moreover, we competed a killing-deficient (T6SS−) variant of the *V. cholerae* strain against other T6SS+ killer strains (four other environmental isolates of *V. cholerae* and *Enterobacter cloacae* [63,64]) to test whether debris accumulation can be independent of the toxins used by different strains (electronic supplementary material, figure S7). In every strain combination, we observed the signatures of killing inhibition due to dead cell debris, i.e. localized dead cell stain (PI) that aligns with both the interface between strains as well as dark outlines in bright-field microscopy.

The evidence presented in figures 1 and 2 suggests that accumulated dead cell debris prevents contact between cells and thus prevents contact killing. However, these data cannot rule out counter-hypotheses such as a change in T6SS gene expression, nutrient density or oxygen concentration. To directly test if the presence of dead cell debris hinders killing, we mechanically disturbed the structural organization of the biofilms and thus broke down dead cell debris barriers, without otherwise altering biofilm conditions (see sketch in figure 3*a*). First, we studied a co-culture of killer and target *V. cholerae* strains. We inoculated the strains at a low initial concentration ($OD_{600} = 1$) between an agar plate and a glass coverslip, and began the measurement after a dense layer of cells formed. Killer cells initially expanded their population; by 3 h, the expansion of killer cells halted (figure 3*b*). After 4.5 h we sheared the biofilm by rotating the coverslip with respect to the agar pad in small circular motions (diameter ~ 2 mm), until both strains and the dead cell debris were well mixed. After the perturbation, we observed an immediate increase in the fraction of killer cells, indicating that killing resumed (figure 3*b*). However, the killer strain took over space almost completely and the remaining target cell domains were too small for us to observe if dead cell debris barriers formed again to separate killer and target cells.

Thus, we performed a new perturbation experiment with two 'mutual' killer *V. cholerae* strains, i.e. each strain was T6SS+ and able to kill the other strain. At 5 h, well after population changes had dramatically slowed (figure 3*d*), we sheared the biofilm (figure 3*e*), thoroughly mixing the two strains and the dead cell debris. After mixing, we observed that large clonal domains again formed over time, indicating that killing had resumed. Further, we observed that these domains became separated by dead cell debris and eventually killing again ceased (figure 3*f*). After shearing and mixing the biofilm a second time (at 19.5 h; figure 3*g*), we again observed the growth of clonal domains that eventually became separated by dead cell debris (figure 3*h*). These findings demonstrate that T6SS killing was prevented by dead

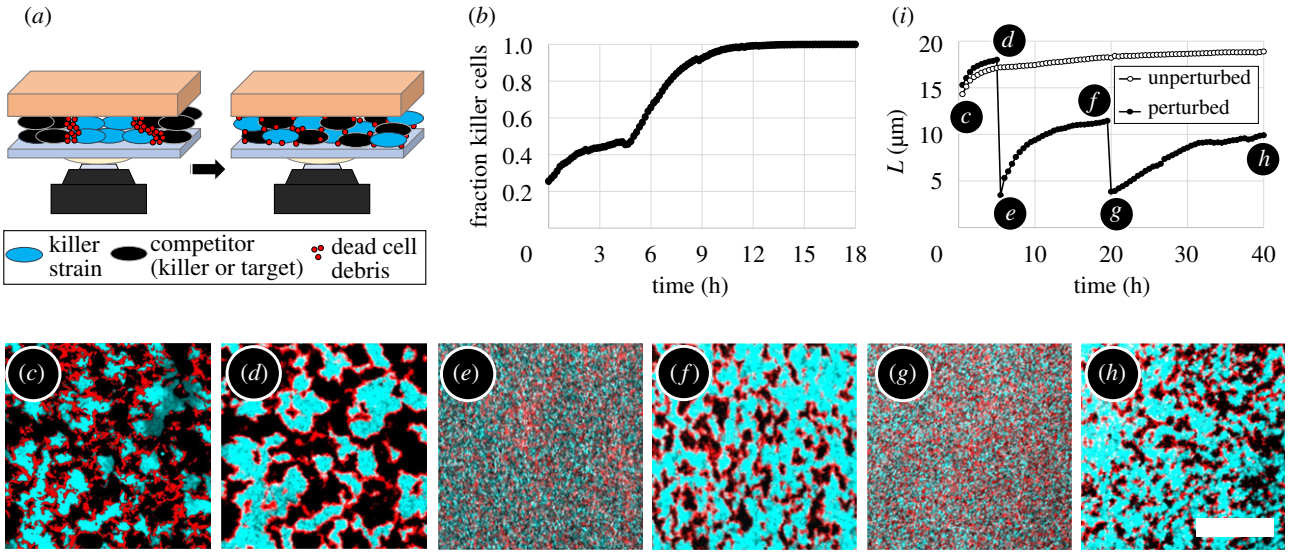

Figure 3. Mechanical perturbation of dead cell debris barriers between domains of competing strains. (*a*) Sketch of mechanical perturbation experiments. The agar pad was rotated against the glass coverslip, mixing both strains and the dead cell debris within the biofilm. (*b*) For unidirectional killing (*V. cholerae* killer against target strain), the fraction of killer cells saturated after an initial increase. After mechanical perturbation at 4.5 h, the fraction of killers increased again as killing resumed, almost eliminating target cells. (See also electronic supplementary material, video 3.) (*c–h*) Time-lapse fluorescence images of mechanical perturbation of a mutual killer biofilm show that phase separation occurred repeatedly: (*c*) after a cellular monolayer has formed, (*d*) before and (*e*) after the first mechanical perturbation at 5 h, (*f*) before and (*g*) after the second perturbation at 19.5 h, and (*h*) the final biofilm structure. In the fluorescence images, one killer strain expresses sfGFP (cyan) while the other killer strain is unlabelled (appears black). In every image, the field of view is densely packed with cells. Dead cell debris was labelled with PI (red). Scale bar (*c–h*): 50 μm. (*i*) The characteristic length, *L*, of domains in mutual killer biofilms increases upon coarsening with time, and abruptly decreases after both mechanical perturbation events. However, *L* increases after each perturbation, indicating that killing resumed (filled circles). In contrast, in unperturbed biofilms *L* plateaus (empty circles).

cell debris barrier formation, and not by other factors such as nutrient depletion or changes in cell behaviour or cell density.

We quantified the growth, and mechanical destruction, of clonal domains by measuring the characteristic length of domains, *L*, of the fluorescent killer strain (figure 3*i*, filled circles) (see electronic supplementary material for details). *L* grows rapidly during the first ~3 h, and much more slowly after that time. Upon the first mixing event, *L* immediately drops to the size of about three cells (figure 3*e*,*g*). After that, *L* increases again, demonstrating that killing had resumed. We obtained a qualitatively similar trend when mixing the biofilm a second time, as indicated by a sudden decrease in *L*, followed by an increase. As a control, we measured *L* for a biofilm that was not mechanically perturbed. The characteristic domain length that emerges after approximately 3 h in the undisturbed biofilm increases by less than 8% over the next 37 h (empty circles in figure 3*h*); in other words, the characteristic length of domains remains nearly constant after initial domain formation has occurred.

2.3. Limited invasion via contact killing

The above results show that the accumulation of dead cell debris can limit the utility of T6SS-mediated killing within biofilms. Contact killing initially eliminates opponent cells, structuring the biofilm population—but only until dead cell debris accumulates and killing nearly ceases. These observations suggest that the T6SS may have limited ability to facilitate biofilm invasion and that completely taking over a biofilm from a small number of T6SS+ cells would be unlikely. To test the ability of T6SS-facilitated invasion, we examined the behaviour of single killer cells in dense environments.

We mixed 1% fluorescent killer cells with 99% non-fluorescent, susceptible target cells, which were otherwise isogenic to the killers. We inoculated and confined an initially dense monolayer of cells ($OD_{600} = 10$) on LB agar pads such that single killer cells were completely surrounded by target cells. We also performed control experiments in which the 1% fluorescent cells were defective killer cells (T6SS–). We found that after 24 h of growth the final killer population was only approximately 1.5× larger than the final fluorescent defective killer control population (figure 4*b*,*c*). In particular, clonal domains of killer cells had a mean size of 18.9 μm^2 (standard deviation of 26.7 μm^2); defective killer control cells formed clonal domains with a mean size of 10.6 μm^2 (standard deviation of 14.9 μm^2). Thus, while killer cells expanded their population more than killing-deficient cells, they were incapable of invading the existing biofilm and eliminating their competitors.

Up to this point, all presented experiments were performed in confinement, i.e. biofilms were grown confined between an agar pad and a glass coverslip, to optimize the set-up for microscopy and exclude height-dependent differences [43,65]. While bacteria often inhabit confined geometries in natural settings [66], it is unclear if confinement itself impacts population dynamics. Thus, we next explored contact killing in unconfined environments, by growing biofilms without a coverslip limiting their height. For both mutual and unidirectional killing, we again observed that the (stronger) killer population rapidly increases for the first 3 h, at which point killing slows substantially (electronic supplementary material, figure S4c,d) and a layer of dead cell debris separates competing strains.

We also repeated the experiments on expansion of active and defective single killer cells in dense environments but

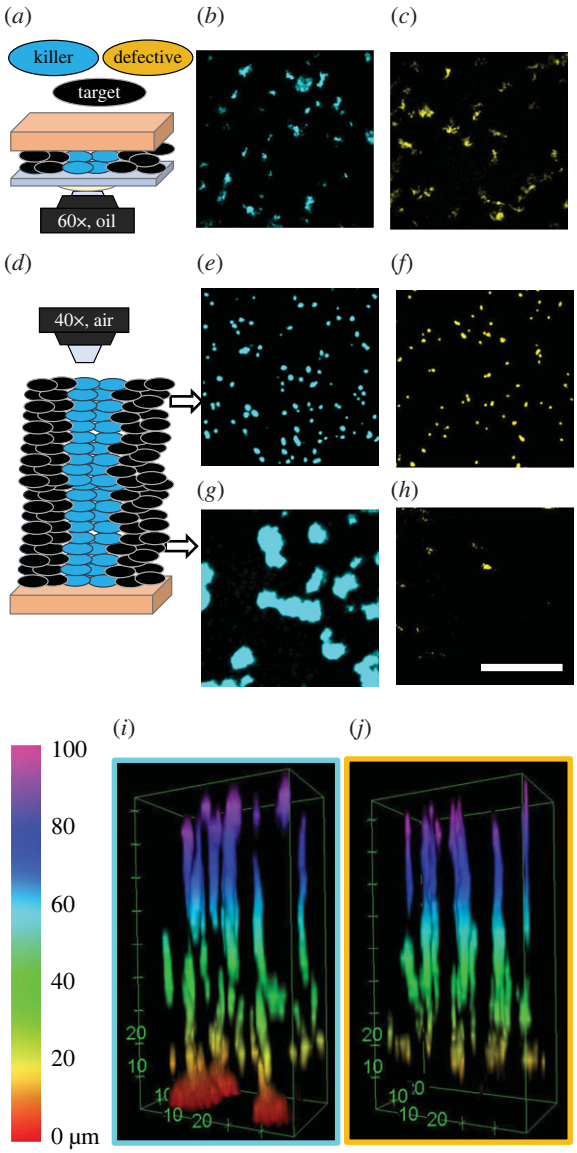

Figure 4. Invasion of dense biofilms by individual cells imaged with confocal microscopy after 24 h of biofilm growth. Biofilms grew from a dense cell monolayer containing 1% fluorescent cells, which were either T6SS+ killer cells (marked blue) or T6SS− defective killer cells (marked yellow). The remaining 99% of the population were non-fluorescent target cells, appearing black. In a confined geometry (schematic in (*a*)), killer cells (*b*) expanded their population only approximately 1.50 times more than defective killer cells (*c*). In unconfined biofilms (schematic in (*d*)) the final abundance of fluorescent cells depended on the distance above the agar surface. At the top of the biofilm, killer cells (*e*) only expanded their population 1.16 times more than defective killer cells (*f*). At the bottom, the killer population (*g*) was 275 times larger than the defective killer population (*h*), which was almost absent. Scale bar *b*,*c*,*e*–*h*: 50 µm. (*i*,*j*) Three-dimensional stack of unconfined biofilms showing that killer (*i*) and defective killer (*j*) cells performed different only within the bottom ∼10 µm. The colour bar indicates the distance from the agar pad.

without confinement. For both killer and defective killer experiments, biofilms reach a height of 92 µm ± 2 µm after 24 h of growth. Similar to the results under confinement, the relative abundances of killer and non-killer control populations differed only slightly (figure 4*i*,*j*): killer strains outperformed non-killer strains by a factor of only 1.64 throughout the whole biofilm. However, we observed that killer and defective killer strains exhibit markedly different behaviour near the agar surface. At the top of the unconfined biofilm, the killer population was only 1.16 times greater than the defective killer population (figure 4*e*,*f*). The mean sizes of clonal domains were 8.0 µm^2 (standard deviation 6.0 µm^2) and 7.4 µm^2 (standard deviation 4.9 µm^2) for killer cells and defective killer cells, respectively. At the bottom of the biofilm (next to the agar surface), some killer cells expanded into large clonal domains (figure 4*g*); the mean diameter of clonal domains of killer cells within 4 µm of the agar surface was 115.4 µm^2 (standard deviation 146.7 µm^2). In contrast, the defective killer cells were nearly eliminated at the bottom (figure 4*h*). (Importantly, the remaining space in figure 4*e*–*h* is occupied by a non-killer strain lacking fluorescent proteins.) In the representative biofilm stacks shown in figure 4*i*,*j*, within 4 µm of the agar surface, the final population of killer cells was 270 times greater than the population of defective killer cells. Thus, although killer cells were only slightly better at invading unconfined biofilms than defective killer cells, killer cells were able to capture territory at the inoculation surface more efficiently.

It is likely that physical effects observed in studies of lateral range expansions [67–70] also play a role in the upward growth of unconfined biofilms. Previous studies found that proliferating cells in crowded environments interact mechanically [71–73], pushing cells towards the expanding cell front. In analogy, during vertical biofilm growth, the few labelled, non-killer cells may be mechanically pushed off the agar surface by neighbouring cells that proliferate. These pushing forces may be diminished near dead cells, which do not reproduce, helping killer cells surrounded by dead cells to remain near the agar surface. In a related vein, it has been shown that rod-shaped bacteria at a solid–liquid interface undergo a mechanically driven transition from planar to vertical orientation during biofilm growth [73–75]. Such a transition probably also occurs in biofilms grown on agar pads. Such cellular reorientations could impact the number and extent of cell–cell contacts, thus altering the kill rate, and may also damage the debris interface. In fact, our time-lapse analysis of unconfined biofilms (electronic supplementary material, figure S4d) shows that the relative abundances of killer cells at the top and the bottom of the biofilm were established during early stages of biofilm growth—when the structural transition probably happens—and remains unchanged afterwards. In a related vein, it was recently reported that cells near the substrate and cells above the substrate behave differently [76], which is consistent with our observations of killer cells at and above the agar surface. However, understanding the roles of mechanical pushing and cellular reorganization in detail would require single-cell resolution experiments, which is beyond the scope of this work.

2.4. Phase separation dynamics

Finally, we analysed the 'coarsening' behaviour of clonal domains during the mechanical shearing experiments (figure 3*c*–*i*). Previous works predicted that the observed phase separation is part of the broad model A, or model A', universality class [24,28]. As a result, the characteristic domain length, L, is predicted to scale as $L \sim \sqrt{t}$ with time t. The mean structure factor, S_L, scales as $S_L \sim t$ [24]. Here, we confirm that killing-mediated phase separation follows these dynamics, despite the accumulation of a dead cell debris barrier (figure 5). Following the analysis in [24], we calculated the Fourier-transformed structure factor, $S(q)$, which provides a measure for the frequency of structure sizes with wavenumber q. We determined the characteristic wavenumber, q_m, as the mean wavenumber q weighted by $S(q)$. From this, we obtained the characteristic domain length, L, which is inversely

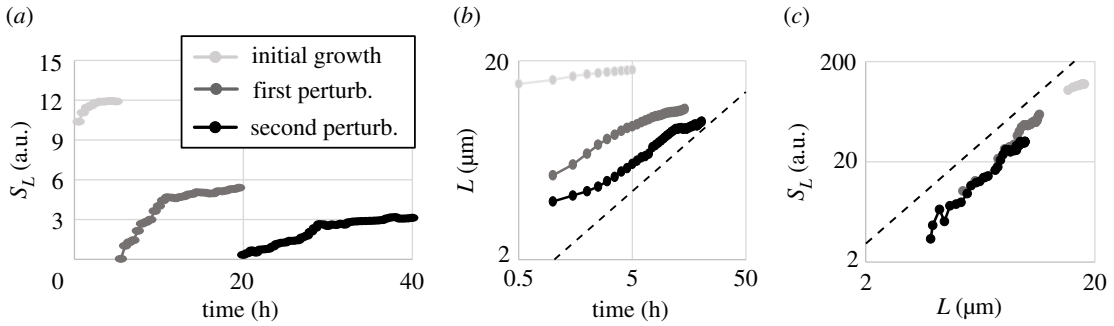

Figure 5. Structural analysis of repeated phase separation during the perturbation experiment in figure 3*c–i*. Time dependence of (*a*) the mean structure factor S_L and (*b*) the characteristic domain length L. (*c*) Time-independent structural analysis, S_L versus L, for each recurrence of coarsening (with same colour code as in (*a*)). Dashed lines indicate the slope that corresponds to model A coarsening.

proportional to q_m, and the mean structure factor S_L, which is the height of $S(q)$ at q_m (see supplementary methods in the electronic supplementary material for details). S_L exhibits linear behaviour each time phase separation occurs (figure 5*a*). However, all three curves exhibit a kink, where the slope decreases by a factor of 31, 9 or 4, respectively. This indicates a change in the speed of domain coarsening, which is probably caused by the establishment of debris barriers. We further found that L approximately follows a square root scaling with time (figure 5*b*) at early times after both perturbation events. However, this scaling analysis depends on when we set time $t = 0$, which is experimentally ambiguous and moreover changes as the speed of coarsening decreases. This ambiguity with respect to time can be avoided by plotting S_L versus L. As predicted, it follows the time-independent, universal scaling of $S_L \sim L^2$ for all data in the mechanical shearing experiment (figure 5*c*).

3. Discussion

Microbial antagonism is common in biofilms [4], and many mechanisms exist that kill on contact. Contact killing has previously been proposed to virtually eliminate susceptible competitor cells of similar numbers within a few hours [9,29,31,77,78] (unless target cells reproduce sufficiently quickly [26]). Surprisingly, we found that killing-induced changes in the target population dramatically slow after approximately 3 h, independent of the initial or final relative abundances of killer cells, and independent of the final amount of contact between competing strains (which varies by a factor of 25 across the different cases explored in figure 1*c*). In fact, even when the T6SS-proficient strain had captured over 99% of the population, small domains of target cells, only a few microns in size, persisted for hours (dashed curve in figure 1*c*).

In this work, we focused on dead cells, finding that the accumulation of dead cell debris is responsible for the observed dramatic decrease in contact killing. By mechanically shearing biofilms, we directly show that killing resumes once dead cell debris barriers are destroyed. Shearing only modifies the positions of cells and dead cell debris, excluding many other hypotheses (such as changes in T6SS gene expression, target cell susceptibility or metabolic activity). We further demonstrate that despite the formation of dead cell barriers the killing-mediated phase separation of competing strains still exhibits dynamics of the model A universality class, which has been predicted previously [24,28].

At first sight, findings presented here might appear to disagree with conclusions drawn from T6SS competition assays, in which T6SS killing decreases the abundance of target cells by several orders of magnitude [7,13,15,29,31]. However, killing competition assays often start with a majority of killer cells over target cells, and the final abundance of target cells has a nonlinear relationship with the initial abundance of killer cells. Decreasing the initial abundance of killer cells leads to enhanced survival of the target cells [23]. This nonlinear phenomenon agrees with our microscopy results; we found that, for the same pair of strains, target inhibition can be as high as 99.97% (three orders of magnitude) or as low as 79.47% (less than one order of magnitude) as the fraction of killer cells during inoculation was varied from 0.50 to 0.09, respectively. In fact, despite the excess of killer cells in competition assays, the target strain is rarely, if ever, *completely* eliminated [7,13,15,29,31]. Previous time-lapse competition assays found that the number of surviving target cells remains remarkably constant after a quick decline in the first few hours [23], consistent with the temporal dynamics we observed via microscopy. Therefore, our observations are in agreement with and explain results from previously reported competition assays. Combined, these results demonstrate that the killing efficiency must be studied and discussed in context, with the initial abundances considered. For example, traditional competition assays show that, for some strains, a large number of killer cells can kill a small number of target cells effectively, but they do not show how a small number of killer cells would perform against a large number of target cells.

Even though the efficacy of killing may be limited by the accumulation of dead cell debris, the utility remains quite high. First, it initially facilitates the formation of clonal domains. Depending on the diffusion length of secreted goods [79], this initial domain formation may be sufficient to favour intra-strain cooperation [24,80,81] or reciprocal benefits between different strains [2,82]. Second, killing can prevent social cheaters from emerging in a population. Such 'policing' effects have been observed in cases where social behaviour is linked with T6SS regulation [83]. Finally, we found that contact-killing strains are able to capture and maintain territory near the surface on which they were inoculated; killing-deficient cells have a much lower probability of remaining near the surface. Occupying nutrient-rich territories may have long-term benefits, beyond the scope of our experiments [84].

The physical inhibition of killing observed here is comparable to other phenomena as seen in contact-dependent growth inhibition experiments [85]. Such a passive defence is starkest in scenarios where the target strain cannot fight back, but the accumulation of dead cell debris eventually prevents killing and protects the target strain from elimination.

Such physical protection stands in stark contrast to active, species-dependent defence mechanisms that are controlled genetically [36,38,40,41]. Physical barriers represent an emergent first line of defence that do not require active sensing or control and are species independent. Other defence mechanisms, e.g. immunity proteins acquired through horizontal gene transfer [86], may help protect small numbers of target cells and become relevant if cells touch directly, before the debris barrier forms or after the debris barrier is broken down.

In this vein, it is important to note that the efficacy of T6SS killing, and thus potentially the role of debris accumulation, can vary among different combinations of strains [87]. In fact, previous measurements demonstrated that the killing ability of *V. cholerae* strains in traditional competition assays can vary by one to seven orders of magnitude [29]. These observations suggest that T6SS killing may be highly effective in some but not all scenarios. The results presented here suggest that the efficacy of T6SS killing also depends on the stability of the cell debris barrier and the rate at which cells can overcome the barrier. The barrier may be broken down through the predation and consumption of dead cells [88], by secreted enzymes (such as lipases or DNases), by shear flow [89] or by other mechanical perturbations, among other potential mechanisms. The rate at which dead cell debris breaks down may also be impacted by the chemical environment and the action of the delivered toxins [87,90], which are known to exhibit a wide range of effects from growth inhibition to lysis [20,21,35,91,92]. Further, while we observed similar characteristics of cell debris accumulation across different co-culture competitions containing *V. cholerae*, *E. cloacae* and *V. harveyi*, the material and physical characteristics of dead cell debris may vary across different combinations of competing strains or species, impacting how long accumulated cell debris prevents contact killing. For example, if competing strains grow at different rates, reproduction may allow the faster growing strain to push through the barrier. Further, motility may enable cells to penetrate barriers as well.

Yet, while several mechanisms may make the debris barrier less stable, dead cell debris is always an obstacle as dead bacteria do not instantaneously disappear. The relative ability or inability of dead cell debris to inhibit contact killing is not a question of if this effect is present, but instead depends on the time scale on which dead cell debris accumulates and how long debris barriers persist. In other words, while the steric hindrance by dead cell debris is likely to be quite general, the impact of debris barriers is specific to the experimental or ecological details [87].

The accumulation of dead cell debris and barrier formation may hold wide-ranging consequences in a variety of contexts. We observe that dead cell debris facilitates the *coexistence* of antagonistic strains, including allowing killer cells to coexist with non-killer strains that cannot fight back. This concept may apply to other modes of microbial killing [4], such as killing mechanisms that act over longer distances via diffusible deadly bio-molecules [93], phages [94] and bacteriocins [95]. These killing mechanisms will typically only be effective within some diffusion length. Killing may thus be hindered if a dead cell debris barrier longer than the diffusion length forms. Moreover, dead cells locally alter the chemical and material composition, promoting biofilm dispersal [96], providing a source of nutrients [97] or protecting against antibiotics [98,99]. Finally, the phenomena we observe are reminiscent of territorial resource competition seen in a variety of ecosystems at various scales [100]. Previous models have suggested that such effects play important roles in maintaining diversity [101,102]. Specifically, the barrier formation we observe is similar to gap formation that occurs during competition between plants [103,104].

In conclusion, it is striking that contact killing indirectly facilitates the coexistence of antagonistic strains [105]. These results suggest that the T6SS, and perhaps other contact killing mechanisms, may not always prompt a microbial 'arms race'. Instead, T6SS-mediated killing may also stabilize diverse communities and the increase in dead cell biomass may facilitate bacterial interaction and survival against external attacks. Further, these results align with recent works which question the ecological purpose of bacterial production of antibiotics [84,106]. Nevertheless, the fact that contact killing facilitates coexistence suggests that the impact of the T6SS in bacterial consortia is complex, and the T6SS is more than simply a potent weapon.

Data accessibility. All experimental datasets are available at https://osf.io/vhmdn.

Authors' contributions. G.S. and P.J.Y. designed the study. C.C. and S.L.N. engineered mutant strains and prepared liquid cultures. G.S. carried out experiments and analysed the data. G.S. and P.J.Y. wrote the manuscript. All authors gave feedback during project development, reviewed the manuscript and gave final approval for publication. P. J. Y. and B. K. H. supervised the project.

Competing interests. We declare we have no competing interests.

Funding. G.S. is grateful for funding from the German National Academy of Sciences Leopoldina (LDPS 2017-03). B.K.H. acknowledges funding from the Gordon and Betty Moore Foundation (grant no. 6790.13), the School of Biological Sciences Abell Fellowship and the College of Sciences Cullen Peck Scholars Award. P.J.Y. acknowledges funding from the Coulter Foundation and the Georgia CTSA. P.J.Y. and B.K.H. acknowledge funding from the NSF Biomaterials (BMAT-2003721).

References

1. Liu W, Jacquiod S, Brejnrod A, Russel J, Burmølle M, Sørensen SJ. 2019 Deciphering links between bacterial interactions and spatial organization in multispecies biofilms. *ISME J.* **13**, 3054–3066. (doi:10.1038/s41396-019-0494-9)
2. Nadell CD, Drescher K, Foster KR. 2016 Spatial structure, cooperation and competition in biofilms. *Nat. Rev. Microbiol.* **14**, 589–600. (doi:10.1038/nrmicro.2016.84)
3. Yanni D, Márquez-Zacarías P, Yunker PJ, Ratcliff WC. 2019 Drivers of spatial structure in social microbial communities. *Curr. Biol.* **29**, R545–R550. (doi:10.1016/j.cub.2019.03.068)
4. Granato ET, Meiller-Legrand TA, Foster KR. 2019 The evolution and ecology of bacterial warfare. *Curr. Biol.* **29**, R521–R537. (doi:10.1016/j.cub.2019.04.024)
5. García-Bayona L, Comstock LE. 2018 Bacterial antagonism in host-associated microbial communities. *Science* **361**, eaat2456. (doi:10.1126/science.aat2456)
6. Aoki SK, Pamma R, Hernday AD, Bickham JE, Braaten BA, Low DA. 2005 Contact-dependent inhibition of growth in *Escherichia coli*. *Science* **309**, 1245–1248. (doi:10.1126/science.1115109)
7. Pukatzki S, Ma AT, Sturtevant D, Krastins B, Sarracino D, Nelson WC, Heidelberg JF, Mekalanos JJ. 2006 Identification of a conserved bacterial protein secretion system in *Vibrio cholerae* using the

Dictyostelium host model system. *Proc. Natl Acad. Sci. USA* **103**, 1528–1533. (doi:10.1073/pnas.0510322103)

8. Nudleman E, Wall D, Kaiser D. 2005 Cell-to-cell transfer of bacterial outer membrane lipoproteins. *Science* **309**, 125–127. (doi:10.1126/science.1112440)
9. Souza DP *et al*. 2015 Bacterial killing via a type IV secretion system. *Nat. Commun.* **6**, 6453. (doi:10.1038/ncomms7453)
10. Bingle LEH, Bailey CM, Pallen MJ. 2008 Type VI secretion: a beginner's guide. *Curr. Opin. Microbiol.* **11**, 3–8. (doi:10.1016/j.mib.2008.01.006)
11. Basler M, Pilhofer M, Henderson GP, Jensen GJ, Mekalanos JJ. 2012 Type VI secretion requires a dynamic contractile phage tail-like structure. *Nature* **483**, 182–186. (doi:10.1038/nature10846)
12. Lin L, Lezan E, Schmidt A, Basler M. 2019 Abundance of bacterial type VI secretion system components measured by targeted proteomics. *Nat. Commun.* **10**, 2584. (doi:10.1038/s41467-019-10466-9)
13. Cianfanelli FR, Monlezun L, Coulthurst SJ. 2016 Aim, load, fire: the type VI secretion system, a bacterial nanoweapon. *Trends Microbiol.* **24**, 51–62. (doi:10.1016/j.tim.2015.10.005)
14. Ho BT, Dong TG, Mekalanos JJ. 2014 A view to a kill: the bacterial type VI secretion system. *Cell Host Microbe* **15**, 9–21. (doi:10.1016/j.chom.2013.11.008)
15. Watve SS, Thomas J, Hammer BK. 2015 CytR is a global positive regulator of competence, type VI secretion, and chitinases in *Vibrio cholerae*. *PLoS ONE* **10**, 0138834. (doi:10.1371/journal.pone.0138834)
16. Zoued A, Brunet YR, Durand E, Aschtgen M-S, Logger L, Douzi B, Journet L, Cambillau C, Cascales E. 2014 Architecture and assembly of the type VI secretion system. *Biochim. Biophys. Acta* **1843**, 1664–1673. (doi:10.1016/j.bbamcr.2014.03.018)
17. Filloux A, Hachani A, Bleves S. 2008 The bacterial type VI secretion machine: yet another player for protein transport across membranes. *Microbiology* **154**, 1570–1583. (doi:10.1099/mic.0.2008/016840-0)
18. Leiman PG, Basler M, Ramagopal UA, Bonanno JB, Sauder JM, Pukatzki S, Burley SK, Almo SC, Mekalanos JJ. 2009 Type VI secretion apparatus and phage tail-associated protein complexes share a common evolutionary origin. *Proc. Natl Acad. Sci. USA* **106**, 4154–4159. (doi:10.1073/pnas.0813360106)
19. Joshi A, Kostiuk B, Rogers A, Teschler J, Pukatzki S, Yildiz FH. 2017 Rules of engagement: the type VI secretion system in *Vibrio cholerae*. *Trends Microbiol.* **25**, 267–279. (doi:10.1016/j.tim.2016.12.003)
20. Crisan CV, Hammer BK. 2020 The *Vibrio cholerae* type VI secretion system: toxins, regulators and consequences. *Environ. Microbiol.* **22**, 4112–4122. (doi:10.1111/1462-2920.14976)
21. Russell AB, Peterson SB, Mougous JD. 2014 Type VI secretion system effectors: poisons with a purpose. *Nat. Rev. Microbiol.* **12**, 137–148. (doi:10.1038/nrmicro3185)
22. Schwarz S, Hood RD, Mougous JD. 2010 What is type VI secretion doing in all those bugs?. *Trends Microbiol.* **18**, 531–537. (doi:10.1016/j.tim.2010.09.001)
23. MacIntyre DL, Miyata ST, Kitaoka M, Pukatzki S. 2010 The *Vibrio cholerae* type VI secretion system displays antimicrobial properties. *Proc. Natl Acad. Sci. USA* **107**, 19 520–19 524. (doi:10.1073/pnas.1012931107)
24. McNally L, Bernardy E, Thomas J, Kalziqi A, Pentz J, Brown SP, Hammer BK, Yunker PJ, Ratcliff WC. 2017 Killing by type VI secretion drives genetic phase separation and correlates with increased cooperation. *Nat. Commun.* **8**, 14371. (doi:10.1038/ncomms14371)
25. Vallespir Lowery N, Ursell T. 2019 Structured environments fundamentally alter dynamics and stability of ecological communities. *Proc. Natl Acad. Sci. USA* **116**, 379–388. (doi:10.1073/pnas.1811887116)
26. Borenstein DB, Ringel P, Basler M, Wingreen NS. 2015 Established microbial colonies can survive type VI secretion assault. *PLoS Comput. Biol.* **11**, e1004520. (doi:10.1371/journal.pcbi.1004520)
27. Kalziqi A, Ng SL, Yanni D, Steinbach G, Hammer BK, Yunker PJ. 2019 Viscosity independent diffusion mediated by death and reproduction in biofilms. (http://arxiv.org/abs/1901.01350)
28. Lavrentovich MO, Nelson DR. 2019 Nucleation of antagonistic organisms and cellular competitions on curved, inflating substrates. *Phys. Rev. E* **100**, 042406. (doi:10.1103/PhysRevE.100.042406)
29. Bernardy EE, Turnsek MA, Wilson SK, Tarr CL, Hammer BK. 2016 Diversity of clinical and environmental isolates of *Vibrio cholerae* in natural transformation and contact-dependent bacterial killing indicative of type VI secretion system activity. *Appl. Environ. Microbiol.* **82**, 2833–2842. (doi:10.1128/AEM.00351-16)
30. Crisan CV *et al*. 2019 Analysis of *Vibrio cholerae* genomes identifies new type VI secretion system gene clusters. *Genome Biol.* **20**, 163. (doi:10.1186/s13059-019-1765-5)
31. Zheng J, Ho B, Mekalanos JJ. 2011 Genetic analysis of anti-amoebae and anti-bacterial activities of the type VI secretion system in *Vibrio cholerae*. *PLoS ONE* **6**, e23876. (doi:10.1371/journal.pone.0023876)
32. Vacheron J, Péchy-Tarr M, Brochet S, Heiman CM, Stojiljkovic M, Maurhofer M, Keel C. 2019 T6SS contributes to gut microbiome invasion and killing of an herbivorous pest insect by plant-beneficial *Pseudomonas protegens*. *ISME J.* **13**, 1318–1329. (doi:10.1038/s41396-019-0353-8)
33. Verster AJ, Ross BD, Radey MC, Bao Y, Goodman AL, Mougous JD, Borenstein E. 2017 The landscape of type VI secretion across human gut microbiomes reveals its role in community composition. *Cell Host Microbe* **22**, 411–419.e4. (doi:10.1016/j.chom.2017.08.010)
34. Coulthurst SJ. 2013 The type VI secretion system—a widespread and versatile cell targeting system. *Res. Microbiol.* **164**, 640–654. (doi:10.1016/j.resmic.2013.03.017)
35. Russell AB, LeRoux M, Hathazi K, Agnello DM, Ishikawa T, Wiggins PA, Wai SN, Mougous JD. 2013 Diverse type VI secretion phospholipases are functionally plastic antibacterial effectors. *Nature* **496**, 508–512. (doi:10.1038/nature12074)
36. Hersch SJ *et al*. 2020 Envelope stress responses defend against type six secretion system attacks independently of immunity proteins. *Nat. Microbiol.* **5**, 706–714. (doi:10.1038/s41564-020-0672-6)
37. Miyata ST, Unterweger D, Rudko SP, Pukatzki S. 2013 Dual expression profile of type VI secretion system immunity genes protects pandemic *Vibrio cholerae*. *PLoS Pathog.* **9**, e1003752. (doi:10.1371/journal.ppat.1003752)
38. Toska J, Ho BT, Mekalanos JJ. 2018 Exopolysaccharide protects *Vibrio cholerae* from exogenous attacks by the type 6 secretion system. *Proc. Natl Acad. Sci. USA* **115**, 7997–8002. (doi:10.1073/pnas.1808469115)
39. Basler M, Ho B, Mekalanos J. 2013 Tit-for-tat: type VI secretion system counterattack during bacterial cell-cell interactions. *Cell* **152**, 884–894. (doi:10.1016/j.cell.2013.01.042)
40. Dong TG, Dong S, Catalano C, Moore R, Liang X, Mekalanos JJ. 2015 Generation of reactive oxygen species by lethal attacks from competing microbes. *Proc. Natl Acad. Sci. USA* **112**, 2181–2186. (doi:10.1073/pnas.1425007112)
41. Lories B, Roberfroid S, Dieltjens L, De Coster D, Foster KR, Steenackers HP. 2020 Biofilm bacteria use stress responses to detect and respond to competitors. *Curr. Biol.* **30**, 1231–1244; e4. (doi:10.1016/j.cub.2020.01.065)
42. Nair HAS, Periasamy S, Yang L, Kjelleberg S, Rice SA. 2017 Real time, spatial, and temporal mapping of the distribution of c-di-GMP during biofilm development. *J. Biol. Chem.* **292**, 477–487. (doi:10.1074/jbc.M116.746743)
43. Wang X, Wang G, Hao M. 2015 Modeling of the *Bacillus subtilis* bacterial biofilm growing on an agar substrate. *Comput. Math. Methods Med.* **2015**, 581829. (doi:10.1155/2015/581829)
44. Wentland EJ, Stewart PS, Huang C-T, McFeters GA. 1996 Spatial variations in growth rate within *Klebsiella pneumoniae* colonies and biofilm. *Biotechnol. Prog.* **12**, 316–321. (doi:10.1021/bp9600243)
45. Xu KD, Stewart PS, Xia F, Huang C-T, McFeters GA. 1998 Spatial physiological heterogeneity in *Pseudomonas aeruginosa* biofilm is determined by oxygen availability. *Appl. Environ. Microbiol.* **64**, 4035–4039. (doi:10.1128/AEM.64.10.4035-4039.1998)
46. Anwar H, Strap JL, Costerton JW. 1992 Establishment of aging biofilms: possible mechanism of bacterial resistance to antimicrobial therapy. *Antimicrob. Agents Chemother.* **36**, 1347–1351. (doi:10.1128/AAC.36.7.1347)
47. Bartolini M *et al*. 2018 Regulation of biofilm aging and dispersal in *Bacillus subtilis* by the alternative sigma factor SigB. *J. Bacteriol.* **201**, e00473. (doi:10.1128/JB.00473-18)
48. Bartolini M *et al*. 2019 Regulation of biofilm aging and dispersal in *Bacillus subtilis* by the alternative

sigma factor SigB. *J. Bacteriol.* **201**, e00473. (doi:10.1128/JB.00473-18)

49. Brooks TM, Unterweger D, Bachmann V, Kostiuk B, Pukatzki S. 2013 Lytic activity of the *Vibrio cholerae* type VI secretion toxin VgrG-3 is inhibited by the antitoxin TsaB. *J. Biol. Chem.* **288**, 7618–7625. (doi:10.1074/jbc.M112.436725)
50. Altindis E, Dong T, Catalano C, Mekalanos J. 2015 Secretome analysis of *Vibrio cholerae* type VI secretion system reveals a new effector-immunity pair. *mBio* **6**, e00075. (doi:10.1128/mBio.00075-15)
51. Dong TG, Ho BT, Yoder-Himes DR, Mekalanos JJ. 2013 Identification of T6SS-dependent effector and immunity proteins by Tn-seq in *Vibrio cholerae*. *Proc. Natl Acad. Sci. USA* **110**, 2623–2628. (doi:10.1073/pnas.1222783110)
52. Hood RD *et al.* 2010 A type VI secretion system of *Pseudomonas aeruginosa* targets a toxin to bacteria. *Cell Host Microbe* **7**, 25–37. (doi:10.1016/j.chom.2009.12.007)
53. Hachani A, Lossi NS, Filloux A. 2013 A visual assay to monitor T6SS-mediated bacterial competition. *J. Vis. Exp.* **73**, e50103. (doi:10.3791/50103)
54. Church SR, Lux T, Baker-Austin C, Buddington SP, Michell SL. 2016 Vibrio vulnificus type 6 secretion system 1 contains anti-bacterial properties. *PLoS ONE* **11**, e0165500. (doi:10.1371/journal.pone.0165500)
55. Ishikawa T, Sabharwal D, Bröms J, Milton DL, Sjöstedt A, Uhlin BE, Wai SN. 2012 Pathoadaptive conditional regulation of the type VI secretion system in *Vibrio cholerae* O1 strains. *Infect. Immun.* **80**, 575–584. (doi:10.1128/IAI.05510-11)
56. Czárán TL, Hoekstra RF, Pagie L. 2002 Chemical warfare between microbes promotes biodiversity. *Proc. Natl Acad. Sci. USA* **99**, 786–790. (doi:10.1073/pnas.012399899)
57. Czaran TL, Hoekstra RF. 2003 Killer-sensitive coexistence in metapopulations of micro-organisms. *Proc. R. Soc. Lond. B* **270**, 1373–1378. (doi:10.1098/rspb.2003.2338)
58. Wong M, Liang X, Smart M, Tang L, Moore R, Ingalls B, Dong TG. 2016 Microbial herd protection mediated by antagonistic interaction in polymicrobial communities. *Appl. Environ. Microbiol.* **82**, 6881–6888. (doi:10.1128/AEM.02210-16)
59. Zepeda-Rivera MA, Saak CC, Gibbs KA. 2018 A proposed chaperone of the bacterial type VI secretion system functions to constrain a self-identity protein. *J. Bacteriol.* **200**, e00688.
60. Wenren LM, Sullivan NL, Cardarelli L, Septer AN, Gibbs KA. 2013 Two independent pathways for self-recognition in *Proteus mirabilis* are linked by type VI-dependent export. *mBio* **4**, 265. (doi:10.1128/mBio.00374-13)
61. Delaney G, Weaire D, Hutzler S, Murphy S. 2005 Random packing of elliptical disks. *Philos. Mag. Lett.* **85**, 89–96. (doi:10.1080/09500830500080763)
62. Donev A, Cisse I, Sachs D, Variano EA, Stillinger FH, Connelly R, Torquato S, Chaikin PM. 2004 Improving the density of jammed disordered packings using ellipsoids. *Science* **303**, 990–993. (doi:10.1126/science.1093010)
63. Stephens WZ, Burns AR, Stagaman K, Wong S, Rawls JF, Guillemin K, Bohannan BJM. 2016 The composition of the zebrafish intestinal microbial community varies across development. *ISME J.* **10**, 644–654. (doi:10.1038/ismej.2015.140)
64. Schlomann BH, Wiles TJ, Wall ES, Guillemin K, Parthasarathy R. 2019 Sublethal antibiotics collapse gut bacterial populations by enhancing aggregation and expulsion. *Proc. Natl Acad. Sci. USA* **116**, 21 392–21 400. (doi:10.1073/pnas.1907567116)
65. Renslow RS, Majors PD, McLean JS, Fredrickson JK, Ahmed B, Beyenal H. 2010 *In situ* effective diffusion coefficient profiles in live biofilms using pulsed-field gradient nuclear magnetic resonance. *Biotechnol. Bioeng.* **106**, 928–937. (doi:10.1002/bit.22755)
66. Bar-On YM, Phillips R, Milo R. 2018 The biomass distribution on Earth. *Proc. Natl Acad. Sci. USA* **115**, 6506–6511. (doi:10.1073/pnas.1711842115)
67. Schreck CF, Fusco D, Karita Y, Martis S, Kayser J, Duvernoy M-C, Hallatschek O. 2019 Impact of crowding on the diversity of expanding populations. *bioRxiv* 743534. (doi:10.1101/743534)
68. Giometto A, Nelson DR, Murray AW. 2018 Physical interactions reduce the power of natural selection in growing yeast colonies. *Proc. Natl Acad. Sci. USA* **115**, 11 448–11 453. (doi:10.1073/pnas.1809587115)
69. Hallatschek O, Hersen P, Ramanathan S, Nelson DR. 2007 Genetic drift at expanding frontiers promotes gene segregation. *Proc. Natl Acad. Sci. USA* **104**, 19 926–19 930. (doi:10.1073/pnas.0710150104)
70. Farrell FD, Gralka M, Hallatschek O, Waclaw B. 2017 Mechanical interactions in bacterial colonies and the surfing probability of beneficial mutations. *J. R. Soc. Interface* **14**, 20170073. (doi:10.1098/rsif.2017.0073)
71. Kalziqi A, Yanni D, Thomas J, Ng SL, Vivek S, Hammer BK, Yunker PJ. 2018 Immotile active matter: activity from death and reproduction. *Phys. Rev. Lett.* **120**, 018101. (doi:10.1103/PhysRevLett.120.018101)
72. Copenhagen K, Alert R, Wingreen NS, Shaevitz JW. 2020 Topological defects induce layer formation in *Myxococcus xanthus* colonies. (http://arxiv.org/abs/2001.03804)
73. Yan J, Sharo AG, Stone HA, Wingreen NS, Bassler BL. 2016 *Vibrio cholerae* biofilm growth program and architecture revealed by single-cell live imaging. *Proc. Natl Acad. Sci. USA* **113**, E5337–E5343. (doi:10.1073/pnas.1611494113)
74. Beroz F, Yan J, Meir Y, Sabass B, Stone HA, Bassler BL, Wingreen NS. 2018 Verticalization of bacterial biofilms. *Nat. Phys.* **14**, 954–960. (doi:10.1038/s41567-018-0170-4)
75. Drescher K, Dunkel J, Nadell CD, van Teeffelen S, Grnja I, Wingreen NS, Stone HA, Bassler BL. 2016 Architectural transitions in *Vibrio cholerae* biofilms at single-cell resolution. *Proc. Natl Acad. Sci. USA* **113**, E2066–E2072. (doi:10.1073/pnas.1601702113)
76. Qin B, Fei C, Bridges AA, Mashruwala AA, Stone HA, Wingreen NS, Bassler BL. 2020 Cell position fates and collective fountain flow in bacterial biofilms revealed by light-sheet microscopy. *Science* **369**, 71–77. (doi:10.1126/science.abb8501)
77. Coulthurst S. 2019 The type VI secretion system: a versatile bacterial weapon. *Microbiology* **165**, 503–515. (doi:10.1099/mic.0.000789)
78. Chen C, Yang XB, Shen XH. 2019 Confirmed and potential roles of bacterial T6SSs in the intestinal ecosystem. *Front. Microbiol.* **10**, 1484. (doi:10.3389/fmicb.2019.01484)
79. Co AD, Vliet Sv, Kiviet DJ, Schlegel S, Ackermann M. 2020 Short-range interactions govern the dynamics and functions of microbial communities. *Nat. Ecol. Evol.* **4**, 366–375. (doi:10.1038/s41559-019-1080-2)
80. Julou T, Mora T, Guillon L, Croquette V, Schalk IJ, Bensimon D, Desprat N. 2013 Cell-cell contacts confine public goods diffusion inside *Pseudomonas aeruginosa* clonal microcolonies. *Proc. Natl Acad. Sci. USA* **110**, 12 577–12 582. (doi:10.1073/pnas.1301428110)
81. Dobay A, Bagheri HC, Messina A, Kümmerli R, Rankin DJ. 2014 Interaction effects of cell diffusion, cell density and public goods properties on the evolution of cooperation in digital microbes. *J. Evol. Biol.* **27**, 1869–1877. (doi:10.1111/jeb.12437)
82. Momeni B, Waite AJ, Shou W. 2013 Spatial self-organization favors heterotypic cooperation over cheating. *Elife* **2**, e00960. (doi:10.7554/eLife.00960)
83. Majerczyk C, Schneider E, Greenberg EP. 2016 Quorum sensing control of type VI secretion factors restricts the proliferation of quorum-sensing mutants. *Elife* **5**, e14712. (doi:10.7554/eLife.14712)
84. Hibbing ME, Fuqua C, Parsek MR, Peterson SB. 2010 Bacterial competition: surviving and thriving in the microbial jungle. *Nat. Rev. Microbiol.* **8**, 15–25. (doi:10.1038/nrmicro2259)
85. Bottery MJ, Passaris I, Dytham C, Wood AJ, van der Woude MW. 2019 Spatial organization of expanding bacterial colonies is affected by contact-dependent growth inhibition. *Curr. Biol.* **29**, 3622–3634; e5. (doi:10.1016/j.cub.2019.08.074)
86. Thomas J, Watve SS, Ratcliff WC, Hammer BK. 2017 Horizontal gene transfer of functional type VI killing genes by natural transformation. *mBio* **8**, e00654. (doi:10.1128/mBio.00654-17)
87. Smith WPJ, Vettiger A, Winter J, Ryser T, Comstock LE, Basler M, Foster KR. 2020 The evolution of the type VI secretion system as a disintegration weapon. *PLoS Biol.* **18**, e3000720. (doi:10.1371/journal.pbio.3000720)
88. Pérez J, Moraleda-Muñoz A, Marcos-Torres FJ, Muñoz-Dorado J. 2016 Bacterial predation: 75 years and counting! *Environ. Microbiol.* **18**, 766–779. (doi:10.1111/1462-2920.13171)
89. Thomen P, Robert J, Monmeyran A, Bitbol A-F, Douarche C, Henry N. 2017 Bacterial biofilm under flow: first a physical struggle to stay, then a matter of breathing. *PLoS ONE* **12**, e0175197. (doi:10.1371/journal.pone.0175197)
90. Unterweger D, Miyata ST, Bachmann V, Brooks TM, Mullins T, Kostiuk B, Provenzano D, Pukatzki S. 2014 The *Vibrio cholerae* type VI secretion system employs diverse effector modules for intraspecific competition. *Nat. Commun.* **5**, 3549. (doi:10.1038/ncomms4549)

91. Durand E, Cambillau C, Cascales E, Journet L. 2014 VgrG, Tae, Tle, and beyond: the versatile arsenal of type VI secretion effectors. *Trends Microbiol.* **22**, 498–507. (doi:10.1016/j.tim.2014.06.004)
92. Yang X, Long M, Shen X. 2018 Effector–immunity pairs provide the T6SS nanomachine its offensive and defensive capabilities. *Molecules* **23**, 1009. (doi:10.3390/molecules23051009)
93. Kohanski MA, Dwyer DJ, Collins JJ. 2010 How antibiotics kill bacteria: from targets to networks. *Nat. Rev. Microbiol.* **8**, 423–435. (doi:10.1038/nrmicro2333)
94. Kortright KE, Chan BK, Koff JL, Turner PE. 2019 Phage therapy: a renewed approach to combat antibiotic-resistant bacteria. *Cell Host Microbe* **25**, 219–232. (doi:10.1016/j.chom.2019.01.014)
95. Scholl D. 2017 Phage tail-like bacteriocins. *Annu. Rev. Virol.* **4**, 453–467. (doi:10.1146/annurev-virology-101416-041632)
96. Mai-Prochnow A, Evans F, Dalisay-Saludes D, Stelzer S, Egan S, James S, Webb JS, Kjelleberg S. 2004 Biofilm development and cell death in the marine bacterium *Pseudoalteromonas tunicata*. *Appl. Environ. Microbiol.* **70**, 3232–3238. (doi:10.1128/AEM.70.6.3232-3238.2004)
97. Schink SJ, Biselli E, Ammar C, Gerland U. 2019 Death rate of *E. coli* during starvation is set by maintenance cost and biomass recycling. *Cell Syst.* **9**, 64–73; e3. (doi:10.1016/j.cels.2019.06.003)
98. Podlesek Z, Butala M, Šakanović A, Žgur Bertok D. 2016 Antibiotic induced bacterial lysis provides a reservoir of persisters. *Antonie Van Leeuwenhoek* **109**, 523–528. (doi:10.1007/s10482-016-0657-x)
99. Auschill TM, Arweiler NB, Netuschil L, Brecx M, Reich E, Sculean A. 2001 Spatial distribution of vital and dead microorganisms in dental biofilms. *Arch. Oral Biol.* **46**, 471–476. (doi:10.1016/S0003-9969(00)00136-9)
100. Wu J, Loucks OL. 1995 From balance of nature to hierarchical patch dynamics: a paradigm shift in ecology. *Q. Rev. Biol.* **70**, 439–466. (doi:10.1086/419172)
101. Weiner BG, Posfai A, Wingreen NS. 2019 Spatial ecology of territorial populations. *Proc. Natl Acad. Sci. USA* **116**, 17 874–17 879. (doi:10.1073/pnas.1911570116)
102. Amarasekare P. 2003 Competitive coexistence in spatially structured environments: a synthesis. *Ecol. Lett.* **6**, 1109–1122. (doi:10.1046/j.1461-0248.2003.00530.x)
103. Liao J, Bogaert J, Nijs I. 2015 Species interactions determine the spatial mortality patterns emerging in plant communities after extreme events. *Sci. Rep.* **5**, 11229. (doi:10.1038/srep11229)
104. Brokaw NVL. 1985 Chapter 4—Treefalls, regrowth, and community structure in tropical forests. In *The ecology of natural disturbance and patch dynamics* (eds STA Pickett, PS White), pp. 53–69. San Diego, CA: Academic Press.
105. Ratzke C, Barrere J, Gore J. 2020 Strength of species interactions determines biodiversity and stability in microbial communities. *Nat. Ecol. Evol.* **4**, 376–383. (doi:10.1038/s41559-020-1099-4)
106. Pishchany G, Kolter R. 2020 On the possible ecological roles of antimicrobials. *Mol. Microbiol.* **113**, 580–587. (doi:10.1111/mmi.14471)